Salisbury
UNIVERSITY

Honor College at Salisbury University

Honors Thesis

An Honors Thesis Titled

Defying Gravity: Design of a Hoverboard

Submitted in partial fulfillment of the requirements for the Honors Designation to the

Honors College

of

Salisbury University

in the Major Department of

Physics

by

Tyler McGraw

Date and Place of Oral Presentation: NCUR, April 10-13, 2019
Kennesaw State University

Signatures of Honors Thesis Committee

	Signature	Print
Mentor:	Matt Bailey	Matt Bailey
Reader 1:	Joseph W Howard	JOSEPH W. HOWARD
Reader 2:		Timothy Stock
Dean:		

Defying Gravity: Design of a Hoverboard

Tyler McGraw

Salisbury University

Author Note

This research was supported in part by funding from the Henson School of Science & Technology summer research fellowship program at Salisbury University.

Contact: tmcgraw1@gulls.salisbury.edu

Abstract

The primary method of transportation for most objects is currently one that relies on friction as the motive force, usually generated by wheels contacting the ground. Necessary contact with the ground for motion not only imposes numerous restrictions on movement but can also prevent traversal of difficult areas entirely. With the design of a hoverboard, there exists the potential for a greater amount of freedom in movement and maneuverability. Ideally such a hoverboard will be designed with the ability to lift at least a 150-pound load, consisting of either a person or cargo. To attempt a hoverboard design that fulfills these requirements as efficiently as possible, aerodynamic theory and mechanics of materials will be combined with a study of existing hoverboard designs and modern advancements in power storage and electric motors.

Defying Gravity: Design of a Hoverboard

The use of friction as the motive force is currently the dominant method of travel and transport from one place to another, by utilization of wheels. The wheels of the transport vehicle push upon the ground of the Earth, and the Earth pushes back with equivalent force following Newton's third law. As the mass of any vehicle is negligible compared to the Earth, and the force applied to both objects will be equal, the vehicle will gain far more acceleration than the Earth and thus be propelled forward. While this is an effective and widely adopted way to move loads, such necessary contact results in many restrictions about how the vehicle can operate. In comparison to a hoverboard, a wheeled vehicle cannot traverse water or stairs easily, and will have significant trouble on any type of rough terrain, such as rocky land that may be covered in sharp objects or potholes. These common issues are solved with the use of a hoverboard, a board that makes transportation possible through interaction with surrounding air, as it has no need to touch the ground and can essentially float over small obstacles without trouble. Perhaps most beneficial of all is the ability for the hoverboard to have complete freedom of movement in any direction desired, including purely vertical climb. However, even the hoverboard will be subject to its own restrictions and requirements for use and will require significant power to operate just like any vehicle. All variables, superscripts, and subscripts used in calculations that follow are denoted and defined in *Table 1*.

Table 1

Variables and Scripts Notation Guide

Variable	Definition
A	Area, in squared units
a	Section lift curve slope, amount of lift generated per increase in angle of attack for a specific airfoil
b	Number of rotor blades
C_D	Drag coefficient, measurement of the resistance of an object to a flow
C_L	Lift coefficient, measurement of the lift generated by an object from a flow moving over it
c	Chord, rotor blade width
c_d	Section drag coefficient, measurement of the resistance of an object to a flow over each infinitesimally small section
c_ℓ	Section lift coefficient, measurement of the lift generated by each infinitesimally small section of an object experiencing a flow
D	Drag, resistance of an object to a flow
E	Modulus of elasticity, the resistance of a material to being temporarily deformed as force is applied
I	Moment of inertia, a measurement of how easily an object will accelerate about a given axis
K	Effective column length factor, determined by the way in which the column ends are supported
k	Kinematic viscosity, the measurement of the extent that a fluid resists flow when not subject to an external force
κ_{ind}	Actual power to induced power ratio
L	Lift, upward force generated by flow over an object or length of an object
M	Mach number, the ratio of a given speed to the speed of sound
P	Power, energy delivered over time or an applied force
R	Rotor blade radius
R_e	Reynolds number, the ratio of internal forces of a flow
r	Radial distance
r_e	Effective radius
r_i	Cutout radius
T	Thrust, a force that propels an object in a desired direction

V	Velocity (constant), or volume
v	Velocity (variable)
W	Weight, the downward force due to the mass of an object
z	Height from a rotor to the ground
α	Angle of attack, angle from the direction of flow to the orientation of the airfoil
θ	Blade section pitch angle, the angle between the airfoil and the rotor disk, on a sectional basis
ϕ	Inflow Angle, the sum of the induced angle by the rotor and the angle due to the rate of climb
ρ	Density of a material, mass for a given volume
σ	Rotor solidity, ratio of rotor blade area to rotor disk area
Ω	Rotor rotational speed
ω	Angular velocity, the rate at which the angle of orientation changes as an object undergoes circular motion

Subscript	Definition
critical	Value at which failure occurs
i	Initial or induced value
ind	Induced value
max	Maximum value
pr	Profile, or shape
r	At radial distance r
t	Tip
tot	Total value
w	Wake

Superscript	Definition
$\bar{}$	Non-dimensional, a unitless value measured relative to a chosen quantity
~	Average value

Note: When variables are combined with subscripts, superscripts, or both, the meanings are combined. For example, θ represents blade section pitch angle by itself, but if written as θ_r, it then represents the blade section pitch angle at a given radial location. If then further written as $\theta_{\bar{r}}$, the blade section pitch angle at a *non-dimensional* radial location is represented.

Aerodynamic Theory

Beginning the design requires an understanding of the source of the vertical thrust that is allowing the board to hover. The thrust from a rotor can be explained through either of two basic principles of physics. The first, Newton's Third Law, states that for any action there is an equal and opposite reaction. In this specific case, while the rotor is spinning, the airfoils, or curved blades, are deflecting the airstream downwards. As a result, by Newton's Third Law, the air must also be pushing upwards in the opposing direction, equal and opposite forces. The second, Bernoulli's Principle, proves that the higher the velocity of a fluid, the lower the pressure. When the pressure in an area drops, the surrounding area that is at a higher pressure pushes inwards to fill the newly created space, forcing the system back into equilibrium. For a spinning airfoil, the shape of the foil is made such that the air has a higher velocity and lower pressure on the top path, causing lower velocity and higher pressure on the bottom path and resulting in the foil getting pushed upwards by the air, creating lift.

With a basic understanding of how a rotor creates lift, which is needed to hover, it is then necessary to move onto aerodynamic theory that models the involved physics and allows for determination of important information that can be used in an actual design. The developmental timeline of aerodynamic theory begins with many assumptions and ideal situations and leads continuously into more complicated and accurate representations of reality. By beginning with the most simplified theory first and working a path through to the most difficult and physically inclusive concepts it is possible to get an initial estimate of possible designs, and then refine the best option into something close to reality.

Momentum Theory

As the one of the first significant aerodynamic theories developed, momentum theory serves to give a quick and easy estimate of the thrust and power requirements relative to a design's specifications. The model used in this theory is ideal and simplified, providing rough estimations at the cost of accuracy. Nonetheless, to check initial feasibility a desired amount of thrust will help to determine the power required for hover, and the necessary size of the rotor(s) providing the lift. For this design the required amount of thrust will at least be equal to the weight of the load that needs to remain in hover. It is important to note at this step that while an equal amount of thrust will indeed sustain the payload in hover, the thrust produced must be able to increase past the weight by a small amount in order to lift the hoverboard and the payload into the air initially. To clarify, the total weight of the hoverboard includes both the hoverboard itself and the payload it is being made to carry. At this early stage, only the payload will be considered, and the mass of the board itself will be temporarily neglected. The desired payload has already been set at 150 lbs, and for the ease of calculation this quantity will be converted into the SI unit of force, newtons ($kg\frac{m}{s^2}$), resulting in about 667N. To proceed further, an understanding of Momentum Theory must be developed to properly use the formulas that will allow for an estimation.

Many assumptions are made for this simplified model as follows: vertical and horizontal flow is assumed to be zero, meaning that the only airflow is caused by the rotor. The rotor is modelled as an infinitely thin actuator disk, where the actuator disk adds energy to the air flowing through it. The flow is inviscid, meaning it has no thickness or internal forces, steady, irrotational, and one-dimensional with no swirl.

There is no flow through the side boundaries of the model, it all remains within. These assumptions allow for a simple model but impose limitations that must be considered with use.

As seen in *Figure 1*, the model can be approached with a combined knowledge of the conservation of mass, energy, and Bernoulli's principle.

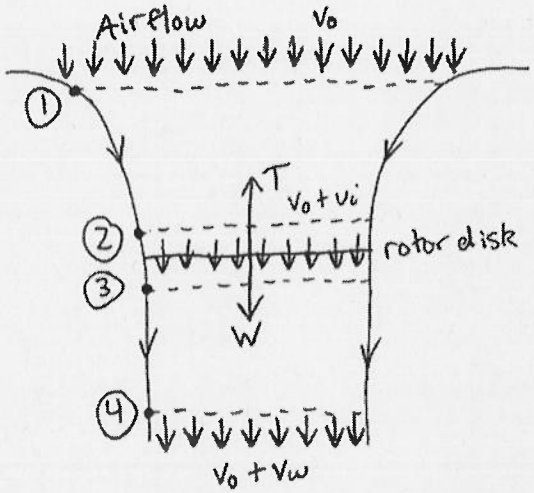

Figure 1. A momentum theory model modified from (Stephniewski 1984), where airflow velocities are illustrated and labeled at four different points, relative to the rotor disk that is adding energy to the flow. The first point represents where the flow enters the model, at an assumed initial velocity of zero for v_0. The second and third points represent the change in velocity across the rotor disk that is adding energy to the flow, denoted as v_i, or the induced velocity. The velocity at points two and three can be proven to be equal by using conservation of mass and Bernoulli's principle. The fourth and final point represents the flow after it is in the far wake of the model, v_w. Thrust and weight are also denoted by T and W respectively.

By using these methods, we can determine an equation

$$P = \sqrt{\frac{T^3}{2A\rho}} \tag{1}$$

that relates thrust (T), power (P), air density (ρ), and rotor disk area (A) (Stephniewski 1984). As a consequence of power, thrust, and area being present in a single equation, to

determine a required quantity the rest of the variables must be turned into constants by choosing values. The amount of thrust needed is already decided and so either power or disk area must be assumed in order to determine the other. To better assist in showing the relation of these variables, as seen in *Table 2*, a spreadsheet easily presents the options. In the interest of keeping the hoverboard as small as possible, a diameter of 4 feet will be chosen as the constant, or about 1.22 meters. This is not an arbitrary decision; by referring to *Table 2* an analysis of the relationship between mass flow rate and power implies that the larger the rotor disk, the larger the mass flow rate, and the lower subsequent power requirement.

Table 2

Momentum Theory Ideal Calculations/Estimates

	Blade Radius	Air Density	Total Weight	Mass Flow Rate	Ideal Power Required
Radius 1	0.3048m	1.225 kg/m^3	667N	21.8 kg/s	20371W
Radius 2	0.3810m	1.225 kg/m^3	667N	27.3 kg/s	16297W
Radius 3	0.4572m	1.225 kg/m^3	667N	32.8 kg/s	13581W
Radius 4	0.6100m	1.225 kg/m^3	667N	43.7 kg/s	10179W
Radius 5	1.0668m	1.225 kg/m^3	667N	76.4 kg/s	5820W

Note: Using equation (1) with a given thrust and air density, the mass flow rate and ideal power can be estimated for a desired rotor blade radius. As the radius increases, ideal power requirements decrease along with an increase in mass flow rate. This implies that larger rotor blades are more efficient, a relationship that is also represented graphically in *Figure 2*.

To summarize this, the larger the rotor blades are the more energy efficient they will be. The relationship between power and rotor disk radius is illustrated in *Figure 2*. While the goal is to make a hoverboard as small as possible while still being able to lift the payload, a balance is necessary to also retain a realistic power draw. Now that an

estimate for the power requirements of the desired thrust has been determined from this simple model, the next step is to include more physical concepts to bring the estimate closer to reality.

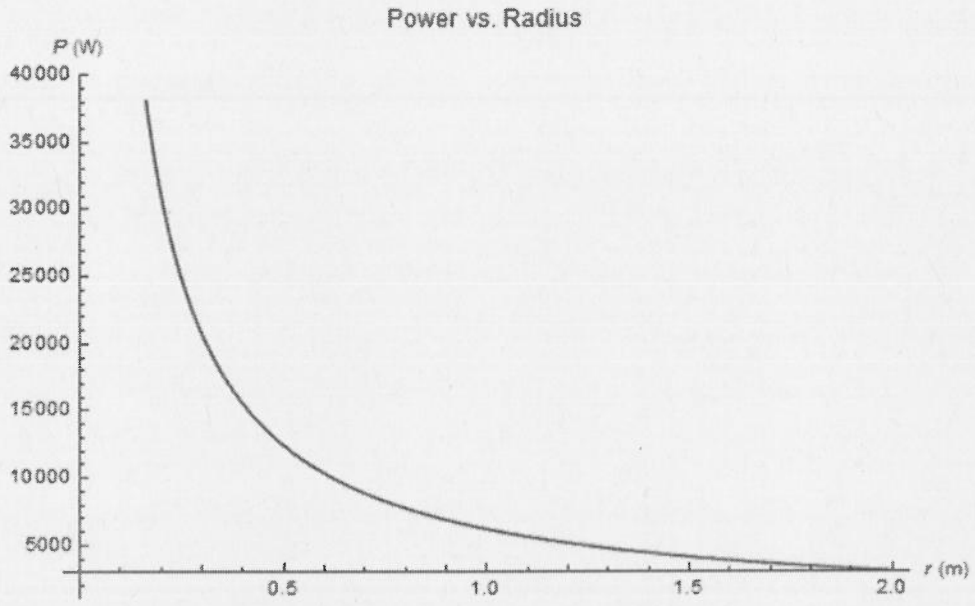

Figure 2. Graph of power required for a desired rotor blade radius, using equation (1), for a given thrust of 667N and air density 1.225 kg per cubic meter. At the chosen radius of 0.61 meters (2 feet), the ideal power required will be 10179W. This point is near the turning point in the graph, a smaller radius causes exponentially larger power requirements, while increases in radius lowers power requirements significantly at the cost of size.

Blade Element Theory

As a more recent development of aerodynamic theory, blade element theory removes more of the assumptions included in the momentum theory model. Blade element theory divides each rotor blade into smaller segments, or blade elements, which allows for integration over the full length. This is an important difference from momentum theory, as the velocity of the airflow over each section of the blade will differ depending on the radius from the center of the rotor. The flow is not actually uniform as

assumed in momentum theory and each blade element experiences a different amount of lift and drag. By integration, these differing values can be summed, and the total thrust, or power, can be determined more accurately.

A representation of this concept of blade integration can be seen in *Figure 3*, where the radius of the blade can be shown as a fraction of the total length, making the quantity non-dimensional.

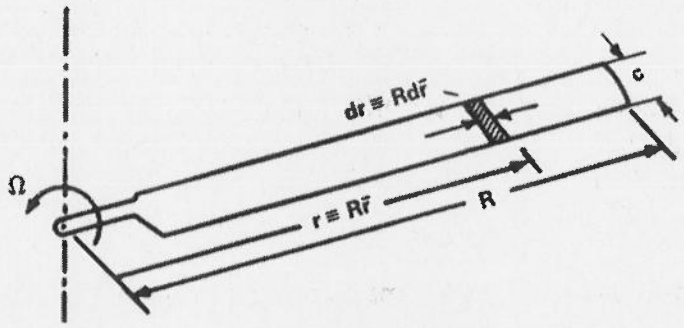

Figure 3. An illustration of the blade station concept, where R represents the total length of the rotor blade. This total length, R, can be multiplied by a quantity, $\bar{r}$, that can vary from 0 to 1. The product of these two provides a nondimensional location at any point along the blade. Also represented in this diagram are c, chord or blade width, and Ω, angular velocity (Stephniewski 1984).

The elementary equations can be written as

$$dL_r = \frac{1}{2} a_r \rho (\theta_r - \frac{v_0 + v_r}{\Omega r}) c_r (\Omega r)^2 dr \tag{2}$$

for lift,

$$dD_{pr_r} = \frac{1}{2} c_{d_r} \rho (\Omega r)^2 c_r dr \tag{3}$$

for profile drag, and finally

$$dT_r = dL_r cos(\phi_r) - dD_{pr_r} sin(\phi_r) \quad (4)$$

for the subsequent thrust that results from knowing the difference between them (Stephniewski 1984). With both quantities known, elementary torque and power can also be subsequently found. These differentials alone include much more information about the interactions of the rotor blades within the model. Where simple momentum theory accounts for only air density, disk area, thrust, and power, blade element theory also includes angle of attack, profile drag, and rotational speed of the rotor, as well as converting many of these quantities into differentials that collectively account for everything happening along the blade.

Blade Element Momentum (B.E.M.) Theory

While both momentum theory and blade element theory model important parts of the rotor interactions, it is not until both theories are combined into one that useful performance predictions can be made (Stephniewski 1984). This combined theory is called blade element momentum theory (B.E.M. Theory). By finding the differential across an elementary annulus (ring shape), seen in *Figure 4*, each individual theory provides a unique differential equation for the change in thrust along the rotor disk radius.

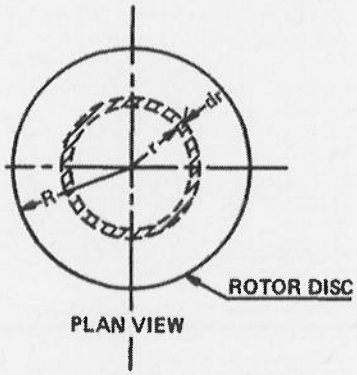

Figure 4. Top down view of an elementary annulus where increments, dr, of the radius can be integrated over the disk to find total values of elements such as thrust (Stephniewski 1984).

From momentum theory, the differential for thrust on the annulus is represented by

$$dT_r = 4\pi\rho v_i(v_o + v_i)rdr = 4\pi\rho v_{\bar{r}}(v_o + v_{\bar{r}})R^2\bar{r}d\bar{r}, \tag{5}$$

where the change in mass flow rate over the differential radius is made dimensionless, by converting dimensional quantities into equivalent expressions (Stephniewski 1984). The corresponding differential that comes from blade element theory is

$$dT_r = \frac{1}{2}c_{\ell_{\bar{r}}}(\Omega r)^2\rho bc_r dr = \frac{1}{2}a_{\bar{r}}\left(\theta_{\bar{r}} - \frac{v_o + v_{\bar{r}}}{\mathrm{v}_t R\bar{r}}\right)(\mathrm{V}_t\bar{r})^2\rho bc_r R d\bar{r}, \tag{6}$$

where the elementary thrust is also considered over a dimensionless radius, the radius at a given fraction of the blade length. Then, by equating the two it is possible to find an equation,

$$v_{\bar{r}} = V_t\left(\frac{-a_{\bar{r}}bc_{\bar{r}}}{16\pi R} + \sqrt{\left(\frac{a_{\bar{r}}bc_{\bar{r}}}{16\pi R}\right)^2 + \frac{-a_{\bar{r}}bc_{\bar{r}}\theta_{\bar{r}}\bar{r}}{8\pi R}}\right) \tag{7}$$

for the induced velocity across the rotor disk at a given radius (Stephniewski 1984). With equation (7), even more information is included as defined variables, also seen in *Table 1*. By accounting for hover conditions, where the intake velocity is assumed to be equal to zero, equation (5) can be re-arranged. Then, after plugging in the ratio of induced velocity to tip speed velocity from equation (7), an expression for the total thrust can be found:

$$T = 4\pi\rho R^2 {V_t}^2 \int_{\bar{r}_i}^{\bar{r}_e} \left(\frac{v_{\bar{r}}}{V_t}\right)^2 \bar{r}\,d\bar{r}. \tag{8}$$

An expression for the induced power of the rotor can be determined easily after the thrust is known, giving

$$P_{ind} = 4\pi\rho R^2 {V_t}^3 \int_{\bar{r}_i}^{\bar{r}_e} \left(\frac{v_{\bar{r}}}{V_t}\right)^3 \bar{r}\,d\bar{r}. \tag{9}$$

However, the induced power is not the only power requirement that must be considered for the rotor. As each airfoil spins it will encounter drag from the airflow, a value that depends upon the airfoils shape and velocity. If the drag on the airfoil increases, the amount of power necessary to continue to rotate through the air will also increase and must be accounted for. This extra power requirement is called the rotor's profile power and can be calculated with

$$P_{pr} = \frac{1}{8}\sigma\pi\rho R^2 {V_t}^3 \tilde{c}_d. \tag{10}$$

By summing the results of equations (9) and (10) together, the total power needed can be found.

Finding the induced velocity across a given radius is very important because it allows for equations (8) and (9) to be completed, which provide accurate estimations for the given thrust and required power respectively. The limits of integration are important to gain this estimate, they define the beginning and ending of the blade over which the elementary quantities are being added up. Typically, the blade will be considered to begin at the end of the blade root cut out, and end at the effective blade length. Blade root cutout is simply a portion of the rotor blade, extending from the center of the rotor, that has been cut out, meaning that the blade does not experience (for the purpose of this model) lift or drag until the end of the cut out has been reached. Besides the convenience of extra room in the design, blade cutout changes also modify the starting Reynolds number at the beginning of the blade base.

The effective blade length is not a physical cut out on the end of the blade, but rather a fraction of the total length that when substituted accounts for tip losses. Tip losses occur from the rotor blades having finite length, meaning that when the air passes over the tip of the blades, vortices are formed that disturb the overall airflow. When the airflow is interrupted in this way, it causes a loss in thrust that can be accounted for by reducing the effective length of the blade. Several methods for finding this effective radius are presented by Stephniewski (1984) and then averaged to a value of 0.952 (95.2% of the radius). For the purposes of this design the effective length will be one, ignoring the effects of tip losses, with the assumption that any rotors used will be ducted, where they are enclosed in an open cylindrical shell. The total effects of ducting the rotor(s) will be further discussed in a later section. A graphical representation of the

thrust calculated with B.E.M. theory can be seen in *Figure 5*, which also illustrates the relative effects of the changes to blade length.

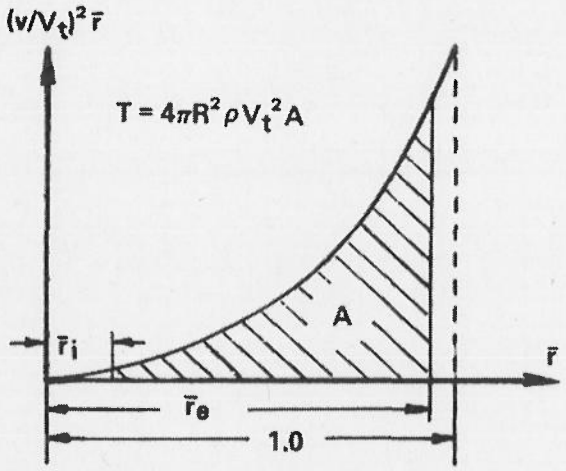

Figure 5. A graphical representation of the integration, equation (8), of the elementary thrust over the entire length of a rotor blade. The integration begins at the blade cutout, r_i, and ends at the effective length, r_e. The area under the curve, A, represents the amount of thrust gained relative to a given blade station $\bar{r}$. The thrust lost by a blade cutout is minimal compared to the large amount of thrust lost due to implementation of an effective length that shortens the blade (Stephniewski 1984).

Reynolds number. Reynolds number can determine the behavior of the airfoil at different lengths of the blade, using

$$R_e = \frac{v_{\bar{r}} c}{k}, \tag{11}$$

where k is the kinematic viscosity of air, measured at 20°C (Anderson 2017). In this specific case the velocity at a radial location will be defined by

$$v_{\bar{r}} = \omega r = \frac{V_t}{R} r, \tag{12}$$

where r is chosen as the desired radial location where the velocity is to be found. This assumes that the airstream velocity across the rotor blade will be similar to the velocity of

the rotor blade itself. Using this process becomes very important when considering integration over the blade length as Reynolds number is not a constant value over the radius of the whole blade. As the radius from the start of the blade increases, so does the Reynolds number. At small values of the Reynolds number, the lift relative to angle of attack (angle of the airfoil relative to the direction of airflow) is much lower and the increase in resulting drag from higher angles of attack occurs much faster. These relationships can be seen in *Figure 6* and *Figure 7*, respectively. By introducing blade cutout, a large amount of unnecessary drag is avoided, power requirements are reduced, and only a negligible amount of thrust is lost in the process.

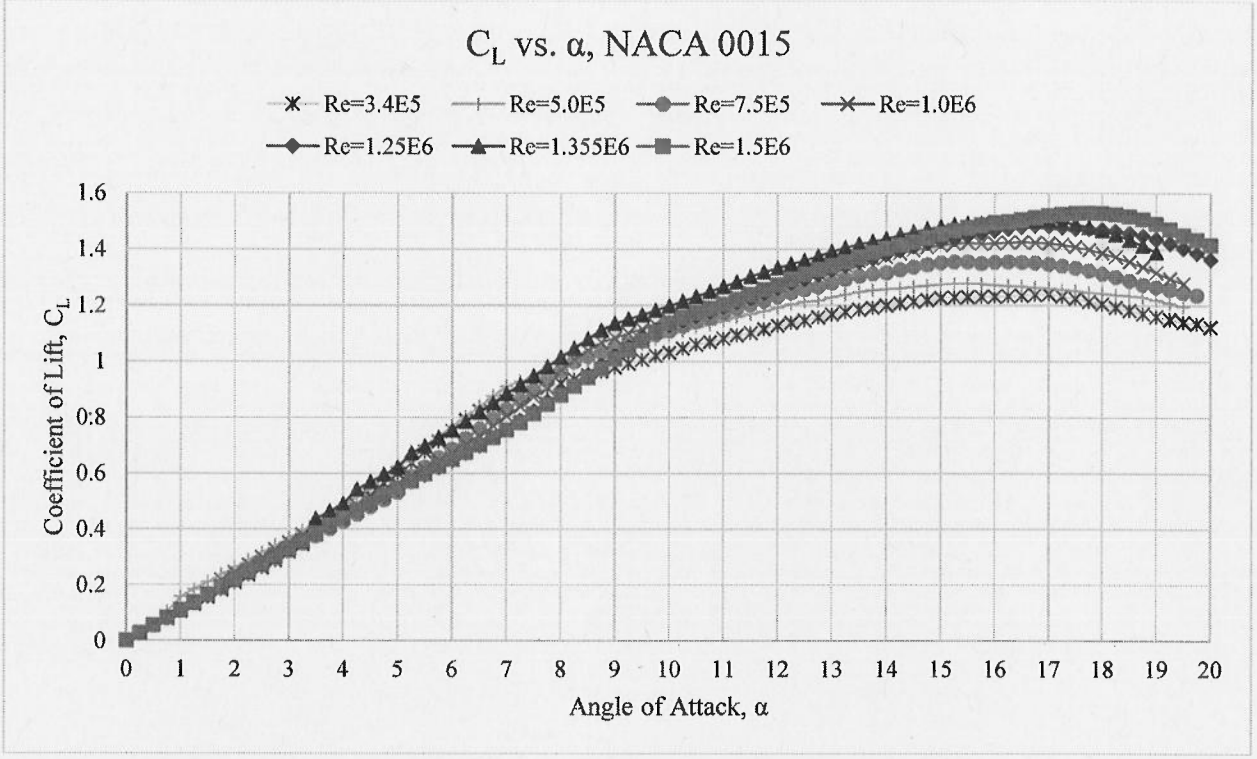

Figure 6. A plot showing the amount of lift the NACA 0015 airfoil is estimated to get relative to the angle of attack that it is oriented at. This airfoil has been chosen due to favorable aerodynamic characteristics that fit the needs of the design. In addition, corresponding data for these characteristics can easily be accessed in many sources from extensive research done in the past. The legend shows the specific Reynolds number (Re) for each series of data points (line), where each is given a unique marker for visibility. Upon inspection, the stall point occurs well after the chosen value of 13 degrees (for all Re experienced by the blade). Each set of lift coefficient values were obtained as an estimate using XFOIL, software that predicts behavior of airfoils with aerodynamic theory (Drela 2013).

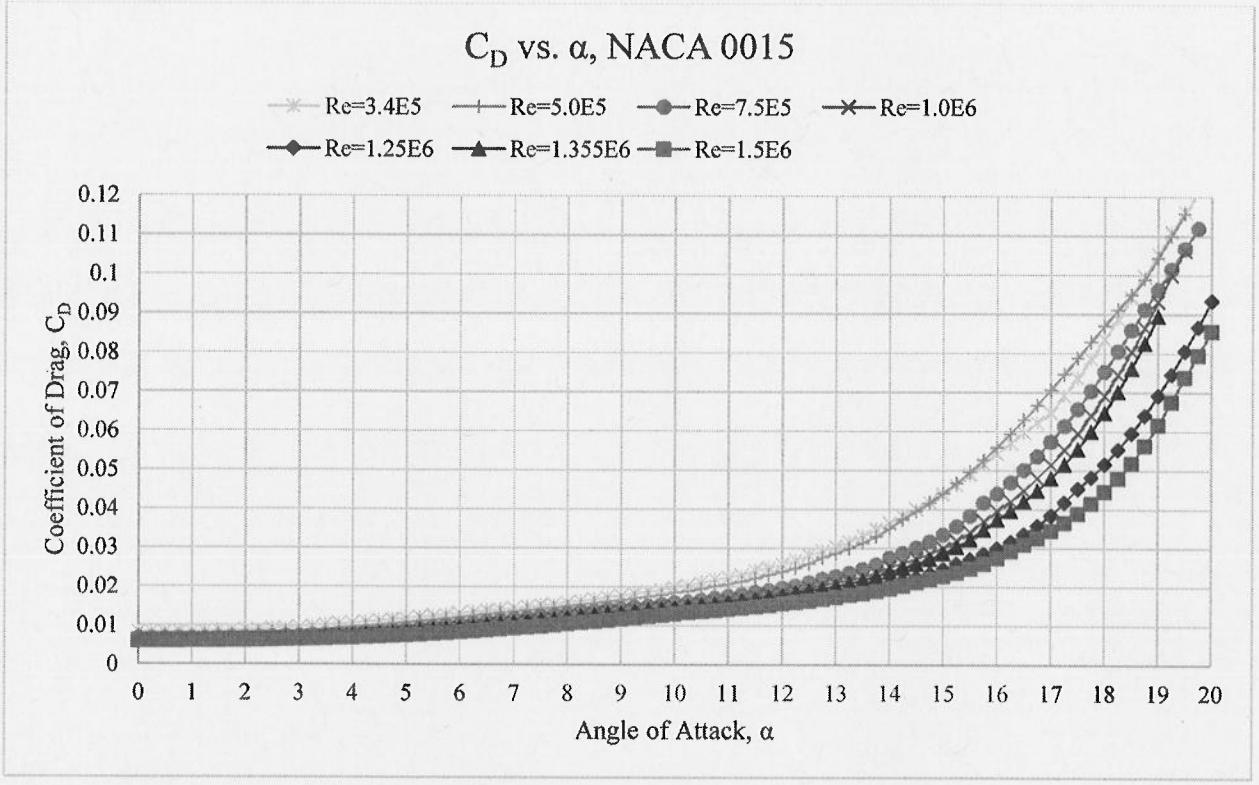

Figure 7. A plot that shows the drag that the NACA 0015 airfoil will experience at a given angle of attack. Unique markers are carried over from the previous figure for consistency, and Reynolds number values are the same. Upon inspection, after a certain α, about 13 degrees (chosen value), the drag increases exponentially. As the Reynolds number increases with the radius of the rotor blade and linear twist decreases the angle, the amount of drag will decrease by a meaningful amount, which subsequently decreases profile power requirements significantly. Each set of drag coefficient values were also estimated using XFOIL (Drela 2013).

Airfoil Selection. The shape of the rotor blades must also be considered, and the lift curve slope, defined as *a*, is the designated variable to include this information. Lift curve slope defines the amount of lift that a given airfoil will experience as the angle of attack increases. As a result of different airfoil shapes providing different amounts of lift and drag relative to angle of attack, it is necessary to find a "sweet spot" where the chosen airfoil for the hoverboard design can provide as much lift as possible at a specific angle while losing as little as possible to drag. The greater the angle of attack, the more

lift will be generated by the airfoil. However, if the angle of attack increases past a certain point the thrust will reach a maximum, where the drag becomes too great for the lift to keep increasing. This is known as the stalling point, where the flow of the air over the airfoil separates from the surface, causing extra vortices in the newly created space and greatly increasing drag. This effect can be seen in *Figure 8*. The selected airfoil for the hoverboard design will be the NACA 0015 (National Advisory Committee for Aeronautics), as it has a desirable lift curve slope and allows for the use of a relatively high angle of attack before drag becomes significant.

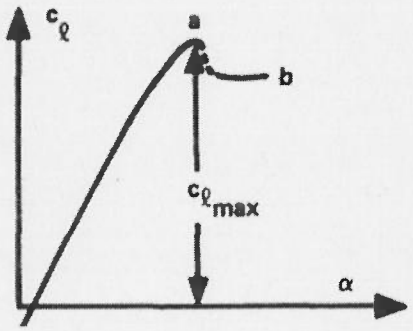

Figure 8. A typical graph of the lift, c_ℓ, versus angle of attack, α, for an airfoil. At point *a*, the lift reaches a maximum, also known as the stalling point, where the lift sharply decreases after continuing to *b* (Stephniewski 1984).

Blade Twist. Linear twist of the rotor blade can be introduced with

$$\theta_{\bar{r}} = \theta_0 \pm \theta_{tot}\bar{r}, \tag{13}$$

which when substituted into equations (8) and (9) with equation (7), defines the amount that the rotor blade angle of attack changes as the radius increases (Stephniewski 1984). By inspection, equation (13) represents two possible equations depending on whether addition or subtraction is chosen, with the change in sign having two distinct effects. By selecting equation (13) with a negative sign, the rotor blades will experience wash-out,

where subtraction indicates that the rotor blades will have the largest angle of attack starting at the base. As the radius increases the angle will linearly decrease to a total chosen amount at the tip, resulting in wash-out. By flipping the sign and changing this equation to addition the rotor blades will instead experience wash-in, which has the opposite effects of wash-out, where the rotor blade will start at a given angle of attack and increase up to a total determined amount. If wash-in is used, the angle of attack along the blades will follow the slope of the lift-drag-angle curve more closely, getting more lift and less drag per degree. However, in this case and many others, wash-out makes a great deal more sense than wash-in even though introducing wash-out effectively decreases the total thrust by a small amount instead of increasing it. As mentioned previously, when the angle of attack increases past a certain point it will hit the stalling point of the airfoil. When this happens there is a significant loss in thrust. Using wash-in, this loss in thrust will occur at the ends of the blades first as they have the highest angle of attack, and thus will stall before any other section of the blade. With wash-out the thrust will instead be lost close to the center of the rotor (effectively where the cutout ends). In comparison, wash-in and the loss in thrust on the edges of the blade may easily cause the entire craft to rotate about axes parallel to the ground, while wash-out will cause a more controlled decrease in altitude with less rotation and more stability.

For a person on the hoverboard especially, wash-in has the potential to make it very hard to remain in operation of the board due to instability and actively changing, unlevel footing. Due to these effects, wash-out will be used for the hoverboard design. The total amount of linear twist will be one degree, small enough to provide stability

benefits while also minimizing the negative impacts upon performance. For the initial angle of attack 13 degrees will be chosen, resulting in 12 degrees at the effective length.

Single Rotor Estimate

With methods now available to calculate the thrust generated from the rotor and the power it will require, it is now possible to develop an early estimate for a single rotor. Although the complete effects of ducting have not been determined and have yet to be discussed at this point, the effective length will be assumed as $r_e = 1$, thereby ignoring tip losses as a result of ducting. This estimate of the single rotor will allow for a comparison of the potential benefits of choosing a coaxial rotor system for the hoverboard versus a single rotor. For consistency, the majority of variable values chosen between coaxial and single rotor configurations will be kept the same to validate comparisons. All chosen constants can be conveniently viewed at once in *Table 3*.

Table 3

Values chosen for determination of thrust and power

Variable	Single Rotor Configuration	Coaxial Rotor Configuration
R	0.61 m	0.61 m
V	235 m/s	178.5 m/s
a	5.73 rad^{-1}	5.73 rad^{-1}
b	2	4
c	0.12 m	0.12 m
θ_{tot}	1°	1°
α	13°	13°
r_i	0.25	0.25
r_e	1	1
$\tilde{c}_d$	< 0.02219	0.02412

Note: The value of $\tilde{c}_d$ will be less than the value given for the single rotor as a result of the Reynolds number being noticeably larger than the highest value represented in *Figure 7*.

Power and Thrust. Due to limitations in power storage and motor efficiency, the power will control the design of the hoverboard. The limit for power that can be supplied to the rotor will be assumed to be around 25.2kW, a cap that will be expanded upon in more detailed when motor selection is discussed. With a restriction on the amount of power that can be spent, it becomes necessary to tweak parameters of the design to gain as much thrust as possible with regards to the power being expended. The nature of the relationship between power and thrust means that the easiest way to increase efficiency is to calculate both values side by side and note the relative effects that changes to each variable results in. Some decisions have effects that can be determined by simple inspection of the equation, while others have more complex interactions with many other

values, making it easier to use the previously described process in some cases for confirmation.

By inspection of equation (9), blade radius and blade tip velocity have the clearest effect upon power. By comparison with equation (8), increasing the blade radius has a similar effect on thrust and power, while increasing the tip velocity contributes far more to increasing power requirements than thrust, a cubic versus square relationship, respectively. This examination further confirms that increasing blade radius is one of the most efficient ways to increase the thrust generated by a rotor while simultaneously keeping power requirements as low as possible. However, as previously mentioned, one of the main goals of the design is to keep the hoverboard as reasonable a size as possible, and so the most effective method to improve efficiency must be ignored in favor of a maximum fixed radius of 0.61m.

The initial angle and linear twist have already been determined previously, as well as the limits of integration, namely the blade cutout and effective length. This leaves only a handful of variables left to determine. One of the simplest is the lift curve slope, as the airfoil chosen is the NACA 0015. A graph of the lift curve slope values for various NACA airfoils can be seen in *Figure 9*, where for the chosen airfoil we get a value of a = 0.1 deg^{-1} = 5.73 rad^{-1}.

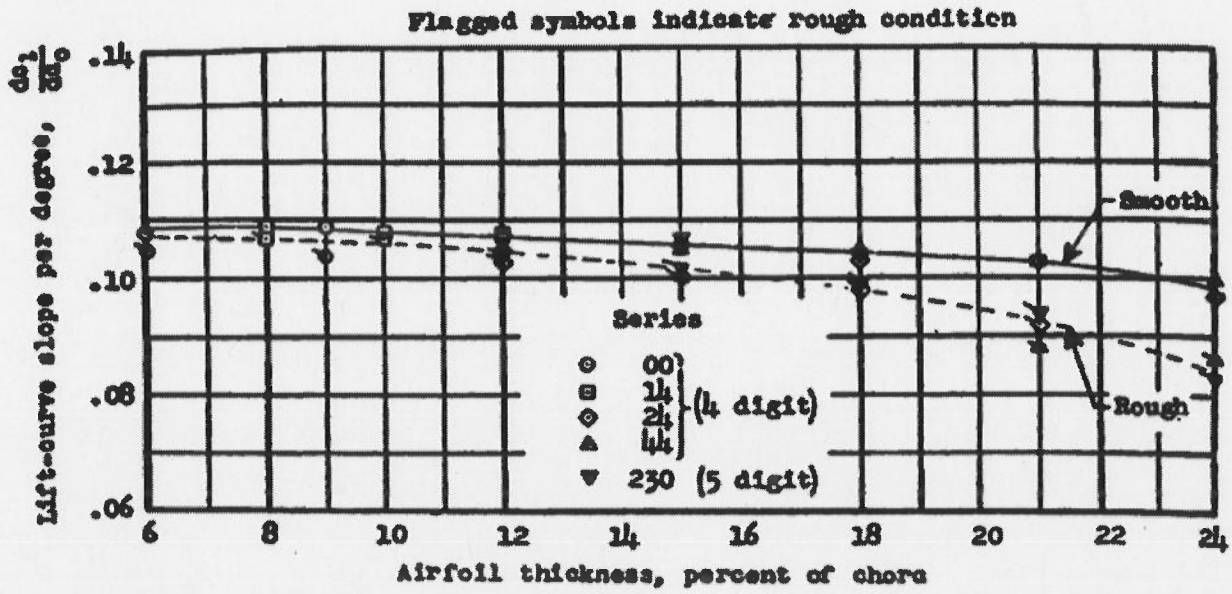

Figure 9. A graph displaying the lift curve slope values for 4 and 5 digit NACA airfoils. Of special interest to the design is the chosen 0015 airfoil, which can be seen to have a value of $a = 0.1$ deg^{-1} = 5.73 rad^{-1} (Abbott 1959). Furthermore, this value is chosen along the rough curve, which reflects reality more accurately as airfoils are not always perfectly smooth in real world applications.

For simplicity the number of rotor blades will be 2, as the solidity, the ratio of the blade area to the rotor disk area, can always be more easily changed using the chord (blade width) value. The chord value that will be used is $c = 0.12$ meters, where it must be noted that changes to the chord will also result in changes to the Reynolds numbers for each blade section. The average section drag coefficient can be obtained by analysis of *Figure 7*. The max value for the drag coefficient will be located at the blade cutout. As the blade radius increases, so too will the Reynolds number, and subsequently the drag coefficient will decrease significantly by the time it reaches the effective length. By adding these boundary values and dividing by two, the average drag coefficient can be determined and used as $\tilde{c}_d \approx 0.2219$. Finally, there is only one variable left, tip velocity, which will can be changed freely until the maximum power is reached, which will also

determine the maximum thrust that can be generated with the chosen parameters. Using this process along with the previously identified values, the maximum power will be P_{max} = 25150W, and T_{max} = 947N, for a single rotor, with $V_t = 235 \frac{m}{s}$.

Considering that the payload limit was defined as 667N, this estimate leaves about 28.5 kg left as a limit for the mass containing the entirety of the hoverboard itself. The tip speed required to achieve this amount of thrust is high, and by relating it to the speed of sound we can find the Mach number with

$$M = \frac{V_t}{343}, \tag{14}$$

where the speed of sound is measured through air that has a temperature of 20°C. Using equation (14), we get that M = 0.685 for the tip velocity of each rotor blade. As this part of the blade is moving the fastest, the rest of the blade can also be assumed to operate in a subsonic fashion. Performing this check is important as once the critical Mach number (M = 1) is approached and exceeded, the flow becomes supersonic instead of subsonic and behaves very differently. For the purposes of this design, the gap is large enough that the airfoil will behave sub-sonically at every radial location. With a single rotor estimate available as a reference, now a second rotor can be included into the design to compare.

Co-axial Rotor Adjustments

Momentum Theory. To incorporate a second rotor, it is simplest to return to momentum theory to determine the effects of the rotors interfering with each other. The model used to conduct this analysis will consist of two *Figure 1* models, except that these models will be stacked on top of one another. An example of this new model can be seen in *Figure 10.*

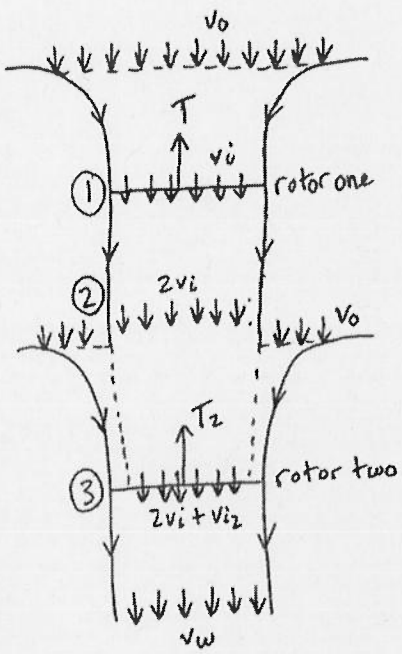

Figure 10. An updated momentum theory model for two rotors in coaxial configuration. This model assumes that the lower rotor is far enough away from the upper rotor that it receives the fully contracted far wake flow from the upper rotor over the inner half of the lower rotor as intake in addition to the lower rotor's own intake on the outer half. Modified version of a model from (Leishman 2006).

By using an analysis similar to the one used on the single rotor model, involving conservation of mass and energy, it can be proven that the lower rotor ends up drawing more power than the upper rotor to provide the same amount of thrust. That is,

$$\kappa_{ind} = \frac{P_{coaxial}}{P_{single}} = \frac{P_{ind}}{2P_{ind}} = \frac{2.5616Tv_i}{2Tv_i} = 1.281, \tag{15}$$

where the ratio of the power draw of two isolated single rotor configurations is compared to the power draw of a single coaxial rotor configuration (Leishman 2006). With this result, the power on the lower rotor is about 56.16% greater than that of the upper rotor. Considering the overall power, the total increase in required power can be taken as a percentage from the induced power factor κ, or, 28.1%. This difference can then be

included into the method previously used in the single rotor estimate by splitting the calculations for the power equation (9), and thrust equation (8), each into one for the upper rotor and one for the lower rotor. The power equation (9) for the lower rotor must then be multiplied by the power gain factor. Additionally, as there are now two rotors experiencing drag instead of one, the profile power, equation (10), will be doubled. By adding these modified equations together, the new results for maximum power and thrust can be found. As with the process for the single rotor estimate, the blade tip velocity will be varied until the max power available is reached. Completing these steps gives P_{max} = 25135W, and T_{max} = 1038N, for a coaxial configuration of two rotors, with $V_t = 174 \frac{m}{s}$.

In comparison with the single rotor estimate, after removing the payload weight, there remains 37.8 kg to contain the hoverboard itself, which is a significant gain of 9.3 kg, equal to about 20.5 lbs. The reason for the slightly lower power and increased thrust can be attributed to the significantly lower blade tip speed. By splitting the total load between two rotors, it allows each rotor to not have to spin as fast to maintain a given thrust.

Initially, the large increase in power requirements for the lower rotor predicted by momentum theory may seem to identify the single rotor configuration as superior, but this result proves the opposite. In fact, the induced power factor estimate for coaxial rotors provided by momentum theory is an overprediction of the value determined by experiment, $\kappa_{ind} = 1.16$ (Leishman 2006). Using this experimentally deduced value will result in an increased power draw of 32% on the lower rotor and 16% overall. Using this experimental factor instead of the theoretical factor then gives even more favorable values of P_{max} = 25157W and T_{max} = 1092N, for $V_t = 178.5 \frac{m}{s}$, further allowing for 5.5

more kilograms to be used for the hoverboard itself after the payload is accounted for, a total of 43.3 kg (95.46 lbs).

Motors & Energy Storage

Motor Selection. As the power requirements of the rotors to generate a given thrust will control the design of the hoverboard, it is necessary to find a motor that can supply a large amount of power to each rotor. As electric motors have much higher efficiency on average in comparison to more traditional engines, only they will be considered in this design. In the single rotor estimate it was noted that the maximum power draw possible will be set at P = 25.2kW. This decision came from the limitations of the chosen electric motor model, which is created by a high-end German electric motor manufacturer Plettenburg. The motor selected is labeled as the Plettenburg NOVA 30/50/4 P50. As with all motors they are subject to an efficiency, that is, when energy is supplied to the motor, the motor can only convert a percentage of the energy into power towards a desired goal. In this case the power is causing the rotation of the rotor blades. For these motors the efficiency varies, but near the maximum power draw of 30kW, the electric motor selected will be around 84% efficiency (Plettenburg Motors). By taking 84% of the max power draw we find that the maximum power that the motor can deliver is 25.2kW, or, the design's power draw limit.

While a single powerful motor makes sense for the single rotor configuration, it would be possible to choose two smaller and weaker motors for the coaxial configuration. Such a decision would also reduce the weight contributed to the design by the motors. However, instead of making this change, two of the selected motors will be used. The reason behind this decision concerns the event of failure of either motor. Including two

powerful motors in coaxial configuration ensures that if one encounters a problem, the other motor (and rotor blades) can provide enough thrust to maintain altitude or at least ensure a slow descent. In comparison with a single rotor configuration, a motor failure would all but guarantee a quick and dangerous return straight to the ground. Furthermore, by being able to keep each motor at under half throttle, the efficiency of the upper and lower motors rises significantly, up to 89% and 90%, respectively (Plettenburg Motors). These values can be found by cross referencing individual rotor power calculations with the electric motor documentation provided by Plettenburg.

Battery Selection. With the electric motors chosen, it is then necessary to provide an energy source (batteries) for them to draw from. In this situation it is most beneficial to choose the highest power density available to maximize energy added per the weight contributed to the hoverboard. Lithium polymer (abbreviated as LiPo) batteries are a commonly used and are an effective method of delivering energy due to their high power density. Specifically, a Tattu 10000mAh LiPo battery pack will be selected due to its relatively high power density compared to other available LiPo battery packs, as well as its ability to be wired in combination for an effective increase in energy and power available.

Some understanding of electrical circuits is necessary to be fully aware of the process needed to convert these batteries into a viable power source for the electric motors. Analysis can be started by converting the specifications of the battery into usable quantities for calculation. The energy contained within the battery is provided in milli amp hours (mAh), which can be converted to watt hours (Wh) with the given voltage of 14.8V per LiPo pack (Tattu LiPo Battery Pack):

$$Watt\ hours = (Amp\ hours)(Voltage) = (10^{-3})(10000\ Ah)(14.8V) = 148\ Wh. \quad (16)$$

Then as the weight of each battery is 0.94 kg, the power density can be found:

$$\frac{148\ Wh}{0.94\ kg} = 157\ \frac{Wh}{kg} \quad (17)$$

Initially, this is a poor power density for a single LiPo battery by itself. Of more importance, however, is the capability of the battery to supply a large amount of energy at once to maintain the power needs of the rotors generating thrust. The power of the battery can be found with

$$Watts = (Amps)(Voltage) = (Discharge\ rating)(Capacity)(Voltage), \quad (18)$$

where amps must be found by multiplying the discharge rating of the battery by its capacity in amp hours. The discharge rating of the selected battery is given as 25C, and so equation (18) gives a power of 3700W per battery. By itself this amount of power also seems low when considering the previously calculated power needs of the hoverboard.

While singular estimates of the battery seem to underperform required specifications, this issue can be resolved by wiring the batteries in a combined configuration of series and parallel. When two batteries are wired in series, the voltage will be summed for each additional battery. When two batteries are wired in parallel, the capacity will be summed for each additional battery. If three pairs of the selected batteries are each placed in parallel and those three sets are connected in series, for a total of 6 LiPo batteries, we then get a total voltage of 44.4V, and a total capacity of 30000mAh. Using equations (16), (17), and (18) with this new configuration results in a higher power density of $236\ \frac{Wh}{kg}$ and a much higher total power supply of 33300W which

satisfies the hoverboard requirements with one of these battery configurations for each electric motor.

Ducting Effects

Incorporating a duct into the hoverboard design provides two major benefits. First, as previously mentioned, the tip losses normally experienced due to the finite length of each rotor blade can be all but eliminated. This effect is achieved by making the inner radius of the duct as close as possible to the length of the blades. As a result, there is not enough space for the detrimental vortices to form as they normal would. Without this interference of the vortices, power requirements are lowered, and consequently it becomes possible to use that extra power gap to generate more thrust if needed.

The addition of a duct can also reduce the power needed to produce a specific thrust, with the effectiveness of the duct being based upon the effects of the chosen duct shape upon the airflow. The less the airflow contracts as a result of the duct, the less power will be required, a relationship of

$$\frac{P_{ducted}}{P_{unducted}} = \frac{1}{\sqrt{2a_w}}, where\ a_w = \frac{v_i}{v_w}, \tag{19}$$

which relates the power of a ducted rotor to an unducted rotor (Leishman 2006). By inspection, the most beneficial outcome will occur when the wake does not contract at all and the ratio of the induced velocity to the wake velocity is equal to one. In this ideal case, the ducted rotor requires about 30% less power to provide the same amount of thrust as an unducted rotor. However, when the ratio is one half, or the ideal contraction predicted with momentum theory, the power required by each system is the same and no benefit is seen. For this reason, an advanced knowledge of fluid dynamics or how a

potential duct design affects the contraction of the airflow, is necessary. Such an analysis is beyond the scope of this thesis, and so it will be assumed that no power reduction benefit is gained from the duct for lack of an accurate estimate.

Ground Effects

When a hovering rotor is near the ground, within a certain range, interference effects can be seen (Leishman 2006). These interference effects result from the ground interacting with the wake from the rotor, which can be seen as either an increase in thrust for a given power, or a reduction in power for a given thrust. Ground effect decreases quickly as the rotor moves straight away from the ground, down to a negligible benefit if the distance of the rotor from the ground exceeds a distance equivalent to one rotor diameter length. For hovering specifically, this relationship is

$$\frac{T_{IGE}}{T_{OGE}} = \frac{1}{1 - (\frac{R}{4z})^2}, \tag{20}$$

where the thrust in ground effect (T_{IGE}) is related to the thrust outside of ground effect (T_{OGE}) (Leishman 2006). From equation (20), as the height from the rotor to the ground, z, increases, the benefit to thrust decreases. When z becomes less than half a radius length of the rotor blade however, equation 18 is no longer valid. The variable benefit to thrust for the hoverboard design can be determined by knowing this range, which starts at about 33.33% when half a radius length away from the ground (0.305 meters) and reduces to only about 1.587% when a full diameter length from the ground (1.22 meters). This means that if the hoverboard is operated within 1.22 meters (4 feet) of the ground a heavier load can be supported, or power requirements will be reduced for a lighter load.

Operation of the hoverboard could still occur outside this range but there would be no additional benefits to efficiency from ground effect.

Structure

With the major components of the hoverboard chosen and the mass allowance known, it is now possible to create a theoretical structure to combine the parts together and check to make sure the limit is not exceeded while also safely supporting flight. The simplest additions to the total mass come from the motors and the batteries that have been chosen, as the masses are provided from the individual manufacturers. Each battery weighs about 0.94 kg, for a total of 12 batteries, and each motor weighs about 6.5 kg max, for a total of two. From the sum of these masses we get about 24.28 kg (53.53 lbs) for the batteries and motor alone. The total height of the hoverboard will be reliant on the necessary spacing of the rotors/motors from the surrounding structure. The ideal spacing for the coaxial configuration can be described by the relationship

$$0.05 \leq \frac{Rotor\ Separation\ Distance}{Rotor\ Diameter} \leq 0.10, \tag{21}$$

where the smallest ratio is an optimal case, and the largest ratio is the typical case (Coleman 1997). Using the optimal ratio, the rotor separation distance in the hoverboard will need to be at least 0.061 meters apart, or about 2.4 inches. By further allotting another inch for the height of each rotor and for the gaps from the rotors to the ends of the duct, we get a total height of about 6.5 inches to use for further mass calculations. As the maximum thickness in a NACA 0015 airfoil will be 15% of the chord length, the assumed inch of height is already larger than the 0.7 inches that the rotor blade could vertically occupy at most, making it a safe assumption.

With the easiest parts of the structure taken care of a handful of slightly more difficult calculations and design choices remain. Namely, masses must be found for the duct, the rotor blades, and remaining support structure to combine these elements into a hoverboard. As the duct will have a large volume, it is important to find a way to retain the functionality of the duct while also keeping the board safe, as well as making the contributed mass as small as possible. To this effect, the duct material will be chosen as carbon fiber so that the large volume has the least impact on the total mass as possible, due to carbon fiber having a low density of about $1700\frac{kg}{m^3}$ (Properties of Carbon Fiber 2018). The remaining frame that will be supporting the duct will be chosen as an aluminum wrought alloy (6061-T6), which has a density of $2710\frac{kg}{m^3}$, a modulus of elasticity of 68.9 GPa, and a yield stress of 131 MPa when subjected to shear (Hibbeler 2017). This information will be important in calculations to determine safety. As technical information about the material properties of carbon fiber is not easily procured, the aluminum will be constructed into an outer frame in such a way that the carbon fiber duct will not be directly subjected to force from the payload.

To find the volume of the carbon fiber duct, the volume of a cylinder will be calculated with the desired thickness of 3 millimeters added onto the radius (chosen to keep volume small),

$$Outer\ Cylinder\ Volume = \pi r^2 h = \pi(1.223m)^2(0.1651m) = 0.7758\ m^3, \quad (22)$$

and then a cylinder with equal height and the radius of the rotor blade length will be subtracted from it,

$$Inner\ Cylinder\ Volume = \pi r^2 h = \pi(1.22m)^2(0.1651m) = 0.7720\ m^3, \quad (23)$$

leaving only an open cylindrical shell (duct) with the volume known:

$$Outer\ Cylinder\ Volume - Inner\ Cylinder\ Volume = 0.0038\ m^3. \quad (24)$$

After multiplying this volume by the density, the mass of the duct will be determined as

$$Duct\ Mass = (0.0038 m^3)\left(1700 \frac{kg}{m^3}\right) = 6.46\ kg. \quad (25)$$

To prevent any part of the duct from buckling due to an unexpected vertical load that may come from a hoverboard operator, an aluminum frame will be implemented. For the calculation of the frame's mass, it will be assumed that the frame is made up of a series of rods. There will be two thin donut shaped rings, one at the top of the duct and one at the bottom. Each of these aluminum rings with have four diameter lengths rods crossing their center at equal spacing, like cutting a circle in half four times. Finally, the rings will be vertically connected at the 8 places that the inner rods meet the rings as well as the middle of those connections, totaling 16 vertical aluminum rods. A representation of this structure can be seen in *Figure 11*. With the necessary material properties known for the aluminum alloy chosen, it then becomes possible to determine the necessary radius of the aluminum rods to prevent failure or excessive bending, as well as the factor of safety. The factor of safety is calculated as the ratio:

$$Factor\ of\ Safety = \frac{Failure}{Allowable}, \quad (26)$$

where failure represents the load that causes unacceptable results such as permanent deformation or buckling, and allowable represents a load smaller than the failure load, related by how large the factor of safety is chosen to be (Hibbeler 2017).

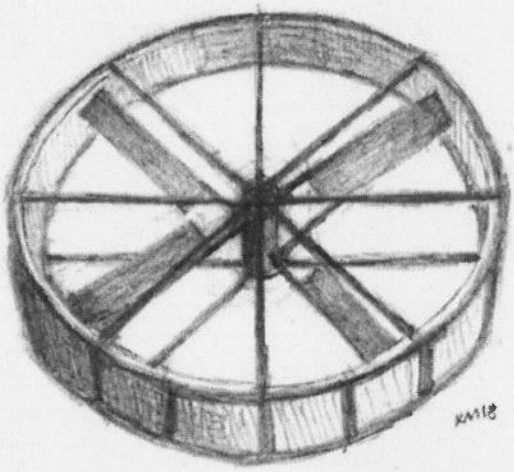

Figure 11. A visual representation of the structure of the theoretical hoverboard, including the frame, duct, and central vertical column from which the rotor blades spin. Used with permission of the artist.

With the aluminum frame supporting the payload there are three distinct possibilities where the rods could fail, shear on the connection of the horizontal rods to the rings, bending on the rings between the vertical rod supports, or buckling of the vertical rod supports. In each calculation the worst-case scenario will be assumed, where the entire payload (667N/150lbs) is being applied to the single point of the frame. In the case of shear, the stress over the rod connection can be related with the yielding stress of the aluminum alloy (131MPa), along with a chosen factor of safety. The yielding stress represents the point at which the aluminum will no longer deform elastically and will begin to deform plastically instead, that is, it will not be able to recover to its original shape and the permanent deformation will likely only increase until failure occurs. By selecting a factor of safety of 2, we can now calculate the necessary rod radius that will sustain the maximum payload without yielding. The factor of safety being 2 essentially means that the rod will be able to support a payload double that (300 lbs) of what should

be applied to it at max (150 lbs). This is to ensure that the hoverboard frame will not experience yielding up a factor of 2 if it is operated in conditions that it was not designed for. By using equation (26) we get

$$2 = \frac{131000000Pa}{\frac{667N}{\pi(r)^2}}, \tag{27}$$

and solving for the radius gives 0.0018 meters (1.8 millimeters) as a minimum radius that can be used to prevent failure by shear at the horizontal rod to ring connections. It will be assumed that connections in the frame will be made by welds that are able to support the full payload without failure. For simplicity, the radius of the rods in each of the sections will be made the same and so whichever minimum radius is the largest will control the design. For the vertical rods connecting the two rings, the minimum rod radius needed for a given critical load can found using

$$P_{critical} = 1334N = \frac{\pi^2 EI}{(KL)^2} = \frac{\pi^2(68900000000Pa)(\frac{\pi}{4}(r)^4)}{((0.5)(0.1651m))^2}, \tag{28}$$

where *r* will need to be at least 0.00203 meters (2.03 millimeters) (Hibbeler 2017). For the bending of the outer ring, the section between vertical rods will be assumed to be a straight beam that is fixed at both ends, allowing for the derivation of an equation for the maximum deflection using known methods for the calculation of displacement by integration (Hibbeler 2017):

$$v_{max} = 0.01 = \frac{PL^3}{192EI} = \frac{(667N)(0.2395m)^3}{(192)(68900000000Pa)(\frac{\pi}{4}(r)^4)}, \tag{29}$$

where r is found to be equal to 0.00306 meters (3.06 millimeters), if the maximum deflection is to not exceed a centimeter. By utilizing equation (29), it can also be determined that the maximum deflection due to bending of the longer rod sections in the rings of the frame will only be less than a centimeter if the radius is increased further to about 6.2 millimeters (6.178 millimeters calculated). At this point the minimum radius found by deflection will clearly control the size of the rods, and so the radius used will be 6.2 millimeters for all rods. The deflection in this area must be smaller than the one-inch gap for safety, if the rod is allowed to deflect too far it will be dangerously close to the rotor blades. With the radius for the aluminum rods determined, the mass for each section of the frame can be calculated, that is,

$$Ring\ Rods\ Mass = (8)(V)(\rho) = 8\pi(0.0062m)^2(1.1952m)\left(2710\frac{kg}{m^3}\right) = 3.13kg, \quad (30)$$

$$Vertical\ Rod\ Mass = (16)(V)(\rho) = 16\pi(0.0062m)^2(0.1403m)\left(2710\frac{kg}{m^3}\right) = 0.735kg, \quad (31)$$

and

$$Ring\ Mass = (2)(V)(\rho) = 2\pi(0.0062m)^2\left(2\pi(0.6224m)\right)\left(2710\frac{kg}{m^3}\right) = 2.56kg, \quad (32)$$

for a total of 6.425 kg of mass for the aluminum frame.

With knowledge of the geometry of the NACA 0015 airfoil, it is possible to estimate a total volume for all four blades, where each motor spins two blades. The simplest method to find this value is to consider a rectangular prism that overestimates the volume by including the entire airfoil shape. For the cross-sectional area of this

rectangular prism, the height will be the maximum thickness of the shape, or 15% of the chord as denoted in the numerical designation for the airfoil (0015), which is 0.018 meters. For the width we simply take the length of the chord, which is 0.12 meters. For the material composition of the airfoil it will be assumed to consist of a foam core inside a carbon fiber shell. By selecting a millimeter thickness for the carbon fiber shell, the outer area will be

$$Outer\ Cross\ Sectional\ Area = (0.020m)(0.122m) = 0.00244m^2, \tag{33}$$

the inner area will be

$$Inner\ Cross\ Sectional\ Area = (0.018m)(0.12m) = 0.00216m^2, \tag{34}$$

and by taking the difference between the two we get the area for the carbon fiber shell:

$$Outer - Inner = 0.00028m^2. \tag{35}$$

Then to find the full volume of the shell, the area from equation (35) must be multiplied by the effective length of all the rotor blades combined. As there is a blade cutout for 25% of the blade, this means that the total blade length will be 75% of the rotor blade radius four times, or 1.83 meters. Using the blade length and the area we find the volume of the carbon fiber shell to be 0.0005124 cubic meters. For the foam core we already have the area present in equation (34), and so multiplying it by the total blade length as well gives us a volume of 0.0039528 cubic meters. A foam called Rohacell A will be chosen for the foam core and has a density of $52\frac{kg}{m^3}$ (Rohacell Foams). As the density of carbon fiber that will be used has previously been determined we can then calculate the respective mass of both the foam core,

$$Foam\ Core\ Mass = (V)(\rho) = (0.0039528m^3)\left(52\frac{kg}{m^3}\right) = 0.2055kg, \quad (36)$$

and the carbon fiber shell,

$$Carbon\ Fiber\ Shell\ Mass = (V)(\rho) = (0.0005124m^3)\left(1700\frac{kg}{m^3}\right) = 0.87kg \quad (37)$$

of the airfoil. Due to the total rotor blade mass being an overestimate it is a reasonable assumption that the actual mass will be under a kilogram, and so this is the mass that will be used.

Now that the masses have been estimated, a final calculation for the total mass of the hoverboard can be found:

$$\begin{aligned} Total\ Hoverboard\ Mass &= 24.28kg + 6.46kg + 6.425kg + 1kg \\ &= 38.165kg. \end{aligned} \quad (38)$$

The only mass measurements not included in this estimate concern the hoverboard central column and connections for the rotor blades and the motors, along with the wiring necessary to deliver power, as the geometry of this area can only be determined with additional research not currently possible for this design due to time constraints. Despite this, it can be safely assumed that any other parts of the structure that remain uncalculated will be small in both volume and mass and therefore should fit within the last 5.135 kg available before the weight limit is reached.

Final Design

With calculations and estimates available for all facets of the hoverboard design, a review can be given of the capabilities and overall viability of the design. Starting with shape, the hoverboard will be a circular and relatively thick disk with a diameter of about

4 feet and a height of about 6.5 inches. In the middle of the circular disk there with be a column that contains two electric motors, which are attached to 2 rotor blades each and spaced evenly from each other (2.5 inches), and from the end of the disk (1-inch gap on each end). The column will be attached on both ends to an aluminum alloy frame consisting of a series of rods connected to two rings. Within the confines of the aluminum frame there will be a thin (3mm) carbon fiber duct that should increase power efficiency by eliminating tip losses, with the potential for even greater benefits the more the duct prevents wake contraction. A visual representation of this physical structure can be seen in *Figure 11*.

The 12 batteries supplying power will be secured on the outer sides of the duct between vertical rods, distributed evenly. While this may pose concern for the potential collision of batteries with obstacles, it is currently the best position where the airflow is not further obstructed. The total mass of the hoverboard for all components then comes out to be about 38.165 kg (84.14 lbs) out of a maximum weight limit of 43.3 kg, which is quite heavy and greatly reduces the portability when not in operation. The payload limit will be up to 68 kg (150 lbs) for either an operator or cargo.

The hoverboard should be capable of providing a total thrust of 1092N (111.3 kg) for about 25.2kW of power, with increases in thrust (or decreases in power consumption) observable when close to the ground up to a height of one diameter length (4 feet). This thrust will be produced by the coaxial rotor configuration where the rotors operate at the same torque but rotate in opposite directions to counteract the effects of the conservation of angular momentum, where the hoverboard itself would otherwise experience rotation opposite to that of the rotors. Furthermore, this configuration provides extra stability from

the large amount of inertia that the spinning rotors will have, making quick rotation about an axis parallel to the ground more difficult (less likely to fall off), and which may also allow for finer kinesthetic control (shifting of weight) of the hoverboard.

With the values of total energy storage and power consumption available it is also possible to estimate the operation time of the hoverboard. For the total energy contained with the batteries we get 9,590,400J, where the energy is measured in joules. The motor will be transferring about 25.2kW of power to the rotors, but to deliver this amount they must take in an even greater amount from the batteries as they are not 100% efficient. These efficiencies as previously mentioned are split, 89% for the upper rotor, and 90% for the lower rotor. Taking these efficiencies into account the motors will need to draw about 28kW in power from the batteries. Finally, by using the power draw and total energy storage just calculated we can see the maximum flight time:

$$Maximum\ Ideal\ Flight\ Time = \frac{9590400J}{28000W} = 342.5\ seconds \approx 5.7\ minutes. \quad (37)$$

This estimate does not include the potential benefits from ground effect, or the extra energy that would be needed to reach an initial altitude (although the quantity would not be significant).

An important caveat of the hoverboard design thus far is that all theoretical calculations have only considered a specific case in which the hoverboard operates **solely in hover without interference from wind**, further research would be necessary to determine the effects of forward flight.

Existing Designs

The creation of a hoverboard is far from being a new endeavor, as many other previous designs have been researched and built. The specifications of each one are relatively unique and each have their own benefits and limitations. By comparing details of other hoverboards with the theoretical hoverboard design that has just been created it is possible to not only see what has been improved upon, but what may yet be made more efficient.

Arcaboard. The Arcaboard is a hoverboard utilizing an array of 36 smaller ducted fans driven by electric motors (Arcaboard). As mentioned by its creators, this allows for the board to keep operating in a reduced capacity even when multiple parts of the system fail. However, having so many individual moving parts will most likely also result in failure more often, requiring additional maintenance. The board is also supplied with energy from a large amount of LiPo batteries, allowing a max flight time of about 6 minutes, similar to the design previously created. The Arcaboard takes the shape of a rectangular prism with a height of 6 inches (vs. 6.5 inches), and dimensions of 1.45 meters by 0.76 meters for an area of about 1.1 square meters, which is not far off from the 1.169 square meters of the previous theoretical design. While the Arcaboard can lift a larger payload of up to 80 kg (176 lbs) for 6 minutes, it can only rise to a height of about 1 foot. This is most likely because the small diameter of the fans used in their design results in a loss of the benefits of ground effect past a relatively small height. Perhaps the most impressive part of the Arcaboard is the composite structure holding the components, which has a mass of only 10 kg (22 lbs), an aspect that has plenty of room for improvement in the theoretical hoverboard design.

Flyboard Air. The Flyboard Air, engineered by Zapata, currently holds the Guinness World Record for farthest hoverboard flight, at 2.252 km (Flyboard Air). This design is by far one of the smallest that currently exists by visual inspection, although dimensions are not specified. Despite this, the board weighs about 20 kg (44 lbs), which is still a great improvement over the created theoretical design. As proven, the Flyboard Air is capable of sustaining flight with a payload of up to 100 kg (220 lbs) for about 6 minutes, utilizing kerosene (jet fuel) for propulsion with multiple turbine engines. While this method of power delivery certainly reduces the size of the board, electric motors are still more efficient at max than turbines using fuel. However, this does allow the flyboard to reach an impressive altitude of 150 meters, well outside any benefits of ground effect, and reach a maximum speed of 140 km/h (87 mph) which is well above speed limits for most roads.

Hiller Flying Platform. Perhaps one of the first hoverboard designs to be researched and built, the Hiller flying platform had many iterations as improvements were made to it over the years. The platform began as a prototype created by NACA (National Advisory Committee for Aeronautics) engineer Charles Zimmerman in the 1950s and developed into much more by the time the U.S. Army awarded him a contract (Hiller Flying Platform). This final model dubbed the VZ-1 Pawnee, is the model that will be reviewed. This platform is one of the largest designs that exists, with a height of 7 feet and diameter of 8 feet. However, lift was generated in a similar way to that of the theoretical design developed in this thesis, utilizing a ducted coaxial rotor setup. The rotors were powered by two or three engines depending on the version, much less efficient than kerosene turbines or electric motors. The weight of the platform alone was

about 180 lbs, which is double the theoretical design developed here, but had a payload of a similar amount.

Omni Hoverboard. Technical information available on the omni hoverboard is limited, but it held the Guinness World Record for farthest hoverboard flight before being surpassed by the Flyboard Air (Omni Hoverboard). The omni hoverboard is perhaps the least safe of the designs, as it has eight small open rotors that appear to be about a foot in diameter each, located at the outside of a small frame. All rotors are also powered by electric motors and LiPo batteries, surely allowing for high efficiency. As a result of the relatively open design, the weight of the board alone is likely small, while still being able to lift a grown man as proven in the video of the record being achieved.

Discussion

With review and comparison of the theoretical design with other hoverboard designs that have been researched and built, some insights can be deduced. Decreasing the mass of the structure supporting the hoverboard appears to be the easiest and most possible improvement. Any reduction in mass could be considered as an increase to the allowed payload, as well as having a large impact on portability. Maximum flight time of a hoverboard in general appears to not exceed about 6 minutes, where the design made is about on par at 5.7 minutes. Acceptable payload varies slightly, but a good goal appears to be around 175 lbs, which improvements in structure could very well provide. The size of the hoverboard also varies widely with other designs, but with the exception of the Flyboard Air, the theoretical design remains at a reasonable size in comparison. The maximum altitude is difficult to determine theoretically, but it can be assumed that the ceiling for ground effect can be reached at minimum, which at 4 feet is enough to avoid

many small ground obstacles. Further comparison is difficult to make without further research into the behavior of the design in forward flight.

For the hoverboard to operate as intended, a few important improvements would be necessary. Maximum flight time at 6 minutes is a relatively short window for operation, this window would have to be increased significantly to be safely considered for use in sensitive situations such as rescue. However, in short periods of operation it would be possible to use the hoverboard to cross difficult sections of terrain that would be resource intensive otherwise, such as a large river. To transport the hoverboard itself without operating it or requiring additional equipment the mass of the structure would have to be greatly reduced, ideally to under 50 lbs, which could be lifted more reasonably. Finally, and most importantly, for any use of the hoverboard it would be necessary for safety to cover the gaps leading to the rotors between the frame at the top of the duct. This would most likely require further research into a mesh that would allow the necessary airflow in with minimal obstruction, but also having material properties that allow it to prevent the operator from falling into the duct and sustaining injuries from the rotor blades.

Conclusions

A theoretical hoverboard design was created with the goal of increasing efficiency over previous hoverboard designs, while keeping in mind safety and accessibility requirements. Aerodynamic theory was utilized to form an accurate estimate of the performance capabilities of the coaxial rotor configuration, which was determined to be superior to a single rotor configuration. According to these estimates, the theoretical design would have enough thrust to lift a 150-pound adult, or cargo, without reaching the

limit of the hoverboard's capabilities. If operated within the range where ground effect would affect the hoverboard, even greater performance could be expected. Additional research into ducting of the coaxial rotors could provide more benefits by changing the ducting shape to reduce power/increase thrust, through reduction in wake contraction. The hoverboard design created does include a duct, but the only benefit from the duct included in calculations is the elimination of tip losses. While the aerodynamic theory used is sufficient to provide an accurate estimate of reality, more advanced aerodynamic theory could provide a more thorough analysis, especially through the use of computational methods.

Existing motors and batteries that best fit the goals of the theoretical design were selected, and the technical specifications provided for each were used to calculate performance. The combined mass of these two components alone contain the majority of the total hoverboard's mass. Therefore, increases in battery power density, or decreases in the motors' material density, would have a significant benefit to the overall design. However, the motors selected do achieve a max efficiency of about 90%, wasting very little energy provided by the batteries to create thrust.

An important downside of selecting LiPo batteries is the relatively long charging time needed before use. For one of the batteries selected, this charging process would take at least a few hours. Therefore, it is reasonable to expect that the hoverboard would have a significantly larger downtime in comparison to its uptime. This means that the utility of using the hoverboard would be most beneficial in situations where the need for convenience in a short (~6 minutes) window, will surpass the cost of preparation time. Scenarios that reflect this kind of need could include emergencies or transportation over

limited stretches of difficult terrain (canyons, rivers, sand, etc.). The hoverboard design, with additional research, could also be used as a method of safe descent from high altitude locations in the event of disaster, where other methods of escape from the location would prove more dangerous. An alternate to the issue of battery power density could be research into the modification of the energy delivery system of the hoverboard, so that it can be wired and used at a stationary site, in an industrial sense, where functions such as cargo transportation would be repeatedly executed.

A knowledge of physics and mechanics of materials was used to plan a physical structure for the hoverboard, with carbon fiber chosen for the duct, and aluminum chosen for a frame encompassing the components. An aluminum frame was necessary to prevent buckling of the carbon fiber duct which might occur if it were exposed to the full payload. The frame will support the load instead of the duct, and was designed to prevent excessive bending and buckling, even in worst case scenarios. While carbon fiber would have been a lighter choice for the frame, the relevant material properties are more difficult to find. The overall weight of the design's structure is currently too high to expect it to be reasonably portable, but with improvements it could be lowered to the point where is it possible to carry over short distances.

Nearly all the goals initially outlined have been met with the theoretical hoverboard design. Detailed research on methods to incorporate the motors into the central column of the hoverboard and inclusion of the subsequent increase in mass is still necessary, as well as design of a mesh covering or other support that would provide a safe and reliable place for the operator to stand without significant risk of slipping into the rotor blades below. For the transportation of cargo this improvement would not be as

vital, as the load could be secured by strapping it to multiple rods. The only case considered thus far for the design is that of the hoverboard hovering in place without interference from wind. Estimations of performance in forward flight and effects from changes in altitude would also be needed to complete the estimation of the design's capabilities. As there is no method for control of the board explicitly stated, it is assumed that the hoverboard would be operated kinesthetically, that is, by the operator shifting their weight to change the direction of the thrust in the desired direction. With these final matters taken care of, the theoretical hoverboard design could then be considered complete.

References

Abbott, I. H., & Von Doenhoff, A. E. (1959). *Theory of Wing Sections*. Dover.

Anderson, J. D. (2017). *Fundamentals of Aerodynamics*. New York, NY: McGraw-Hill Education.

Arcaboard. (n.d.). Retrieved November 15, 2018, from http://www.arcaspace.com/en/arcaboard.htm

Coleman, C. P. (1997). *A Survey of Theoretical and Experimental Coaxial Rotor Aerodynamic Research* (pp. 1-34, Tech. No. 3675). Moffett Field, California: NASA Ames Research Center.

Drela, M., & Youngren, H. (2013, December 23). XFOIL - Subsonic Airfoil Development System. Retrieved October, 2018, from https://web.mit.edu/drela/Public/web/xfoil/

Flyboard Air. (n.d.). Retrieved November 15, 2018, from https://zapata.com/air-products/flyboardair

Hibbeler, R. C. (2017). *Statics and Mechanics of Materials* (Fifth ed.). Pearson.

Hiller Flying Platform. (n.d.). Retrieved November 15, 2018, from https://www.hiller.org/event/flying-platform/

Leishman, J. G. (2006). *Principles of helicopter aerodynamics*. Cambridge: Cambridge University Press.

Omni Hoverboard. (n.d.). Retrieved November 15, 2018, from http://omnihoverboards.com/

Plettenburg Motors. (n.d.). Retrieved November 14, 2018, from https://www.plettenberg-motoren.net/en/products/motor-solutions/motors

Properties of Carbon Fiber. (2018). Retrieved November 14, 2018, from https://www.clearwatercomposites.com/resources/properties-of-carbon-fiber/

Rohacell Foams. (n.d.). Retrieved November 15, 2018, from https://www.rohacell.com/product/rohacell/en/products-services/

Stephniewski, W. Z., & Keys, C. N. (1984). *Rotary-Wing Aerodynamics: 2 volumes bound as one*. Dover.

Tattu LiPo Battery Pack. (n.d.). Retrieved November 14, 2018, from https://www.genstattu.com/tattu-10000mah-14-8v-25c-4s1p-lipo-battery-pack-without-plug.html